Published online June 28, 2005

Quantifying Pore-Size Spectrum of Macropore-Type Preferential Pathways

K.-J. S. Kung,* M. Hanke, C. S. Helling, E. J. Kladivko, T. J. Gish, T. S. Steenhuis, and D. B. Jaynes

ABSTRACT

Structural pores associated with macropore-type preferential flow pathways can accelerate chemical transport in unsaturated soils, thereby potentially causing groundwater contamination. To predict chemical transport through these pathways, classical deterministic models depend on soil hydraulic conductivity, which effectively lumps flow contributions from all individual pathways. We contend, however, that quantifying the pore spectrum of preferential pathways, without lumping the contributions of individual pores, is the appropriate method for simulating convective chemical transport through macropore-type preferential pathways. In this study, we conducted field-scale experiments by using an improved tile drain monitoring protocol to measure the mass flux breakthrough patterns of conservative tracers. The tails of these patterns suggested that the impact of preferential pathways on contaminant transport can be conceptualized as that occurring through cylindrical capillary tubes. We then proposed a distribution function bracketed by sharp cut-off points to represent the pore spectrum of these tubes. Finally, we used the measured tracer breakthrough curves (BTCs) as data sources to find the parameters of the proposed function. Our results, based on the best fitting, showed that the preferential pathways are naturally clustered into domains; preferential pathways with a wide range of pore radii could become active simultaneously when infiltration rate increases. Because the derived pore spectra simultaneously satisfy both water movement and solute transport, pore spectra can be used to (i) calculate soil hydraulic conductivity of preferential pathways in deterministic approaches, and (ii) construct multiple probability density functions (PDFs) for the transfer function approach, to accommodate different infiltration patterns.

The soil's capacity to store water and nutrients facilitates the hydrological and biogeochemical cycles critical for the existence of terrestrial ecosystems. This capacity hinges on the porous nature of soils. Natural soils have a spectrum of pores with radii generally ranging from 10^{-3} to 10^{-7} m. The smaller soil matrix pores are comprised of textural voids among the soil primary particles, while the larger pores are often made of structural voids among the soil secondary structures. The matrix pores are always interconnected and usually self-similar. Large secondary structural pores are likely to exhibit more complexity. Their formation is dictated by physical (e.g., shrinking and swelling, wetting and drying, or freezing and thawing) and biological (e.g., penetration and movement of living organisms) forces (Bouma, 1981; Gish and Jury, 1983; Edwards et al., 1993). Both physical and biological processes have temporal and spatial patterns of formation and destruction cycles (Gupta et al., 2002). Tillage practices and compaction, for example, often destroy the continuity of large structural pores (Isensee et al., 1990). The coefficient of variation of soil hydraulic conductivity, which is often dictated by the soil structural pores, ranged from 100 to 400% (Libardi et al., 1980; Warrick and Nielsen, 1980). This suggests that the spatial variability of soil structural pores measured by using core- or block-sized samples is very large. As a result, the size spectrum of large structural pores measured at several random locations by small sample sizes in a field may not represent the spectrum of the entire field. Temporal extrapolation of measurements may be similarly invalid. For these reasons, it is difficult to directly measure the field-scale spectrum of the large structural pores, yet this property is among the most important soil properties when dealing with issues related to water quality.

Soil characteristic curves and hydraulic conductivity curves were used in past research from the 1950s and 1960s [summarized by Hillel (1980, p. 183–185) and Jury et al. (1991, p. 89–94)] to quantify the soil pore-size distribution. However, because these curves were typically measured using homogenized soils where the larger soil structural pores were destroyed, these earlier approaches only addressed the matrix pore spectrum among primary particles after homogenization. Later, intact soil samples such as soil cores or blocks were used; however, even intact samples cannot capture the variability and continuity of field-scale, large secondary structural pores (Shipitalo and Edwards, 1993).

Large structural pores can contribute to macropore-type preferential flow, and field experiments confirmed that flow via such pathways bypassed the far-more-prevalent soil matrix pores to cause rapid and deep chemical leaching (Germann and Beven, 1981; Luxmoore, 1991; Helling and Gish, 1991). Kladivko et al. (1999) showed that >50% of the total annual pesticide loss generally occurred during the first major precipitation event of >25 mm rain after pesticide application. Fast breakthrough patterns of adsorbing chemicals through macropore-type preferential flow resembled those of conservative nonadsorbing chemicals (Kladivko et al., 1999; Kung et al., 2000b; Fortin et al., 2002). In analogous cases, deep leaching of P through preferential transport was found, even though P loss is assumed to occur mainly by surface runoff (Hergert et al., 1981; Stamm et al., 1998; and Beauchemin et al., 1998). Beside agrichemicals, pathogenic microorganisms such as fecal coliforms and

K.-J.S. Kung and M. Hanke, Dep. Soil Science, Univ. of Wisconsin-Madison, Madison, WI 53706-1299; C.S. Helling, Sustainable Perennial Crops Lab., and T.J. Gish, Hydrology Lab., USDA-ARS, BARC-W, Beltsville, MD 20705-2350; E.J. Kladivko, Dep. Agronomy, Purdue Univ., West Lafayette, IN 47907; T.S. Steenhuis, Dep. Biological and Environmental Engineering, Cornell Univ., Ithaca, NY 14850; D.B. Jaynes, National Soil Tilth Lab., USDA-ARS, Ames, IA 50011. Received 25 June 2004. *Corresponding author (kskung@wisc.edu).

Published in Soil Sci. Soc. Am. J. 69:1196–1208 (2005).
Soil Physics
doi:10.2136/sssaj2004.0208

677 S. Segoe Rd., Madison, WI 53711 USA

Abbreviations: 1-D, one-dimensional; BTC, breakthrough curve; CDE, convection–dispersion equation; PDF, probability density function; PFBA, pentafluorobenzoic acid; *o*-TFMBA, *o*-trifluoromethylbenzoic acid.

viruses (Geohring et al., 1999; Woessner et al., 1998), and antibiotic and hormonal compounds from animal wastes (Rodvang and Simpkins, 2001), have been transported through preferential flow, thereby causing groundwater contamination.

Some lab-scale mapping methods have been developed to accurately measure pore sizes and connectivity of macropore-type preferential pathways (Anderson et al., 2002). However, no instrument is currently available to directly measure the pore spectrum of field-scale, macropore-type preferential pathways. Based on long-term observations from field experiments, tile-drained plots actually serve as huge intact lysimeters, integrating total leaching; therefore, a tile-sampling protocol should be superior to soil coring or suction lysimeter methods for examining the impact of field-scale macropore-type preferential pathways (Kung et al., 2000a; Kladivko et al., 2001; Zehe and Flühler, 2001; Fortin et al., 2002). Nevertheless, these studies were conducted under transient conditions, where lateral movement of water and chemical among adjacent pathways induced by matric potential gradient would enhance hydrodynamic dispersion. To accurately quantify pore spectrum of preferential pathways, dispersion must be minimized.

Under steady-state conditions, all hydraulically active pathways are saturated and could be considered as independent pathways where water movement and chemical transport through each pathway has minimum interaction with those in adjacent pathways. In this scenario, the BTC of a short chemical pulse is the summation of all BTCs of individual pathways. This suggests that tracer BTCs measured under different steady-state infiltration conditions could serve better to quantify the pore spectrum of preferential pathways. On the basis of a tile drain monitoring method developed by Richard and Steenhuis (1988), Gish et al. (2004) measured tracer breakthrough patterns under two steady-state conditions by applying chemical in a narrow strip, parallel and offset to a tile line. They found that, at a 0.89 mm h^{-1} steady-state infiltration rate, tracer arrival time and peak flux time were approximately 90 and 250 h after application, respectively, and tracer mass flux pattern could be fitted perfectly by a one-dimensional (1-D) analytical solution of the convection–dispersion equation (CDE). They concluded that preferential pathways were not active at this infiltration rate. However, when steady-state infiltration rate was increased to 4.4 mm h^{-1}, they found that the tracer was detected in tile drainage only 16 min after application (Fig. 1) and the breakthrough pattern had a very early broad peak. This suggested that (i) there was a threshold, beyond which preferential flow pathways became hydraulically active, and (ii) active preferential pathways had a wide spectrum of pore radii. A similar trend was observed by Seyfried and Rao (1987).

The objective of this study was to quantify the field-scale pore-size spectrum of macropore-type preferential pathways at different infiltration rates. To explain how this goal was accomplished, the rest of the paper has two main sections. First, how field experiments were conducted to measure BTCs of conservative tracers under two different long-term, steady-state infiltration rates and what were the major findings were described in the Materials and Methods and Results sections, respectively. Then, a theory was proposed to conceptualize and quantify the spectrum of preferential pathways by using the BTCs as surrogate data sources in the Theory section. Finally, we provided a Discussion to compare our approach with previous chemical transport approaches.

MATERIALS AND METHODS

Field experiments were conducted at the Walworth County Farm in Elkhorn, WI. The research site is located within the Southern Wisconsin and Northern Illinois Drift Plain with Pella silt loam soil (fine-silty, mixed, superactive, mesic, Typic Endoaquolls). The tile drain research facility consists of tiles spaced 18 m apart at a depth of 0.9 to 1.1 m. Two irrigation sheds were used, the long side of each shed being parallel to, and offset 0.3 m from, the center tile line. Within each shed, water was applied through eight calibrated nozzles, 2.4 m apart, and mounted on a trolley that oscillated along the length of the shed. This design offered high Christiansen uniformity of water application to a 2.7- by 19.2-m area inside the shed under all climatic conditions. The layout of tile monitoring procedure, the irrigation design, and soil properties were described in detail by Gish et al. (2004) and Hanke et al. (2004).

Three tracer experiments were conducted: two in autumn 2001 and one in spring 2002. In 2001, the long-term steady-state irrigation rate of the first experiment was 1.2 mm h^{-1}, and 1000 g pentafluorobenzoic acid (PFBA) dissolved in 15 L of water was applied through the irrigation system. The irrigation rate of the second 2001 experiment was 2.4 mm h^{-1}, and 500 g *o*-trifluoromethylbenzoic acid (*o*-TFMBA) dissolved in 15 L of water was applied. In 2002, the irrigation rate was again 2.4 mm h^{-1}, with application of 686 g PFBA dissolved in 14 L of water. There was no residual PFBA detected in tile drain in spring 2002. These tracers were chosen because they are conservative and have nearly identical transport properties as bromide in many soils (Jaynes, 1994; Kung et al., 2000a). [Data from an earlier experiment conducted by Gish et al. (2004) are also included in the overall analyses of tracer mass flux breakthrough patterns in our paper. This study was conducted on the same Wisconsin site, using the same techniques, but at 4.4 mm h^{-1}.]

The volumetric flow rate of tile drainage was continuously monitored by using a submerged pressure transducer to measure water height in a flume with a 15° v-shaped, sharp-edged notch. Two days after tile flow reached steady state under a certain infiltration rate, a short pulse of a conservative tracer was applied through the irrigation system to the area inside the shed, where a valve controlled the water source (either from a tracer tank or from tap water). Water samples were collected manually from the tile drain once every 2 min during the first 2 h and then by samplers every 6 min for the next 10 h after tracer application to detect the initial tracer breakthrough. The sampling interval gradually increased to every 2 h by the fourth day and was maintained at that interval until approximately 25 d after each tracer application.

RESULTS

On the basis of the measured tile flow rate and tracer concentration in the tile flow, mass flux of each tracer recovered from the tile drain was calculated and normalized by the mass of each tracer applied. In the 2.4 mm h^{-1} infiltration study, tracer arrival was detected at approximately 8 to 10 h after tracer application (or after

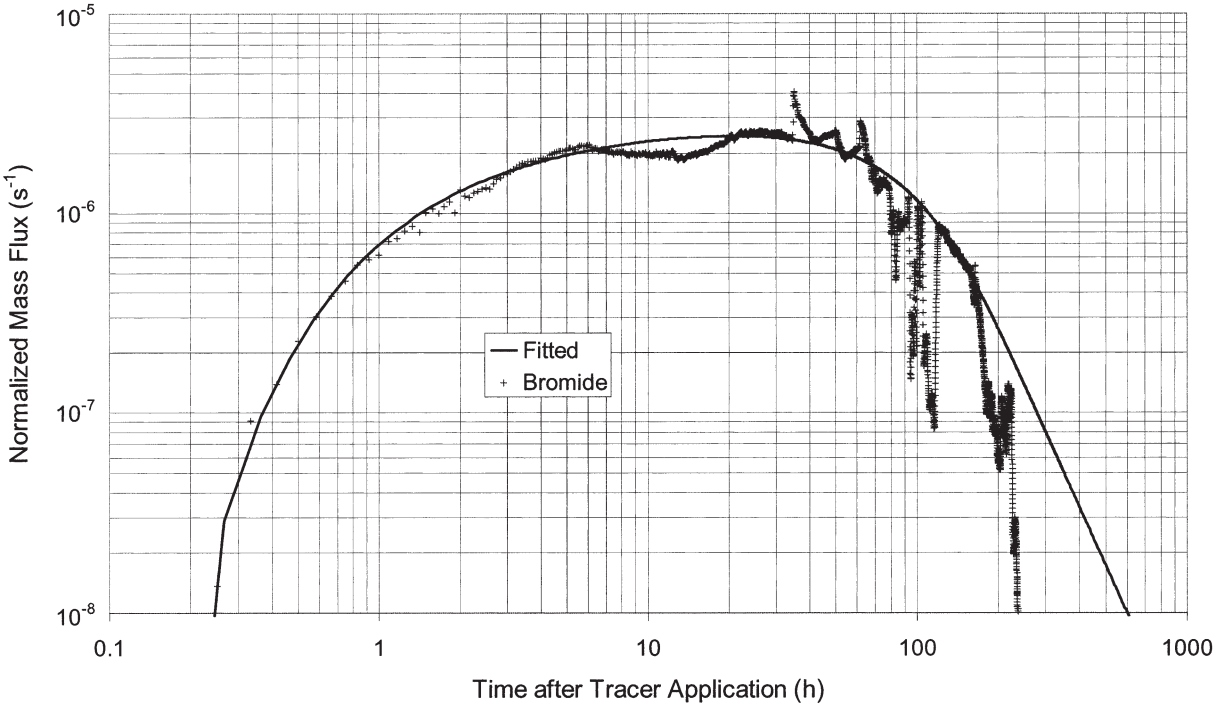

Fig. 1. Bromide breakthrough curve from tile drain under a 4.4 mm h^{-1} steady-state irrigation rate (from Gish et al., 2004). Calculated curve is best fit of Eq. [5] to data.

19–24 mm of irrigation); tracer mass flux peaked between 75 and 100 h after tracer application (Fig. 2). By comparison, under the 4.4 mm h^{-1} steady-state infiltration rate (Fig. 1 from Gish et al., 2004), the tracer arrived only 16 min after its application (or after 1.2 mm of irrigation). Because the arrival time of a conservative tracer is dictated by pore sizes of pathways in which the tracer is transported, these results suggest that many preferential pathways with larger pore radii are not hydraulically active when infiltration rates decreased from 4.4 to 2.4 mm h^{-1}.

To use tracer breakthrough patterns as surrogates to quantify the pore spectrum of preferential pathways, an area large enough to encompass the spatial variability of

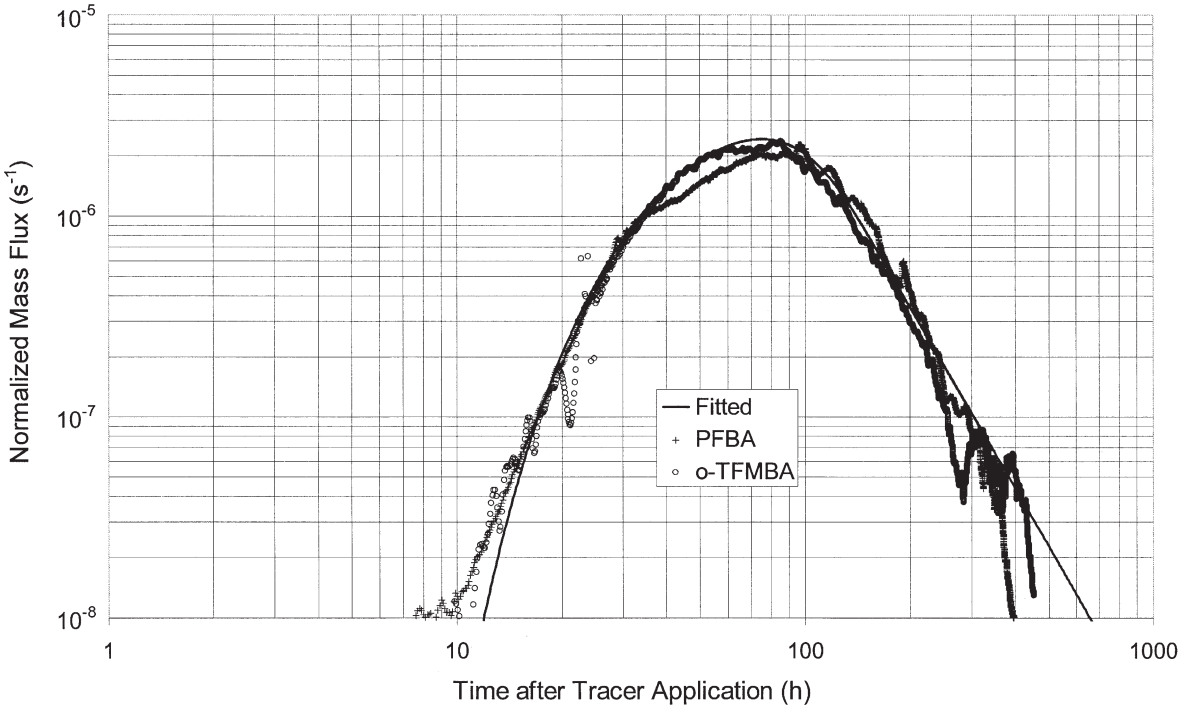

Fig. 2. Tracer breakthrough curves from tile drain under a 2.4 mm h^{-1} steady-state irrigation rate. The *o*-TFMBA (*o*-trifluoromethylbenzoic acid) experiment was conducted in autumn 2001, while the PFBA (pentafluorobenzoic acid) experiment was conducted in spring 2002. Calculated curves are best fit of Eq. [5] to data.

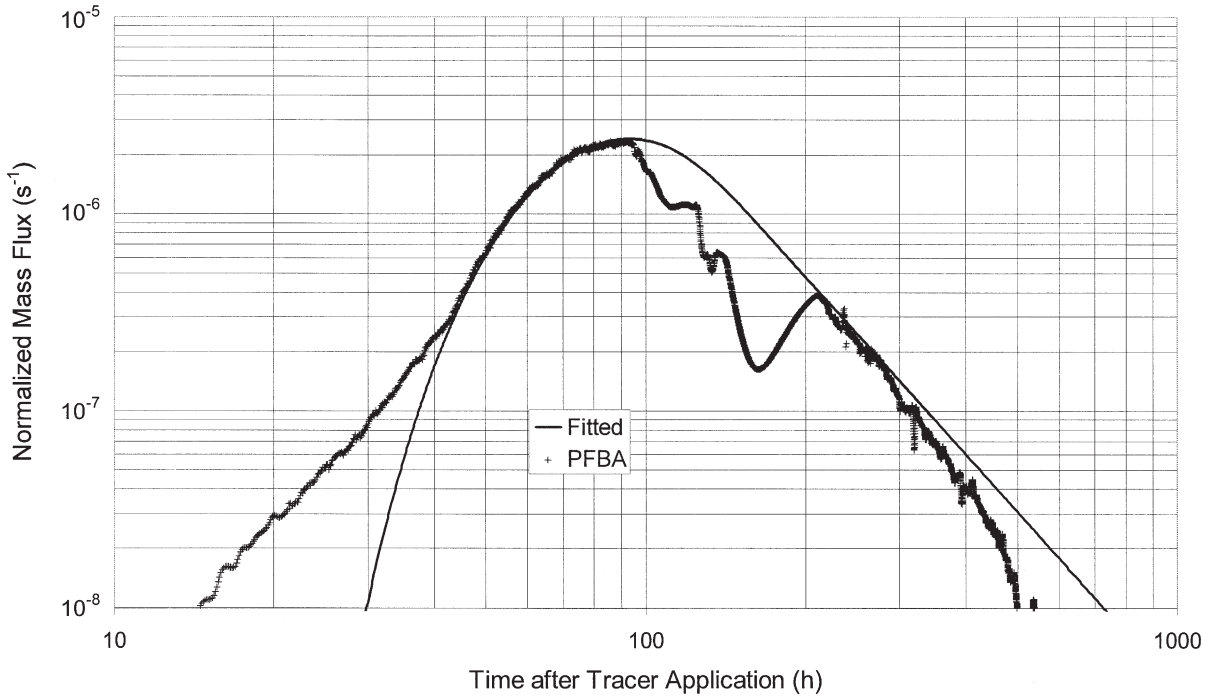

Fig. 3. Pentafluorobenzoic acid (PFBA) breakthrough curve from tile drain under a 1.2 mm h^{-1} steady-state irrigation rate. Calculated curve is best fit of Eq. [5] to data.

the field-scale preferential pathways should be chosen. However, from the literature, the representative area to sample field-scale preferential pathways is undefined. Published results addressing the impact of preferential flow on contaminant transport had significant fluctuations and variability (Shaw et al., 2000; Williams et al., 2003). Figure 2 shows that two replicated tracer BTCs at 2.4 mm h^{-1} are very similar. The mass recoveries of *o*-TFMBA and PFBA are 87.6 and 90.3% of that applied, respectively. The *o*-TFMBA experiment was conducted after corn harvest in autumn 2001; the PFBA was conducted in the same field before soybean planting in spring 2002. Soil temperature at 30 cm dropped below 0°C four times during the 2001–2002 winter. The close match of two replicated BTCs indicates that (i) the 2.7 × 19.2 m experimental area is representative enough to capture the field-scale spatial and temporal variability of preferential pathways, at least at the 2.4 mm h^{-1} rate, and (ii) the field-scale preferential flow pathways persisted after several freeze–thaw cycles.

Results from the 1.2 mm h^{-1} irrigation are shown in Fig. 3. The PFBA tracer arrived at ≈14 h and peaked at ≈90 h after tracer application. This again suggested that, as infiltration rates decrease from 2.4 to 1.2 mm h^{-1}, fewer preferential pathways remain hydraulically active. Deflections in the BTCs are explainable anomalies, reflective of the difficulties in conducting long-term, steady-state field experiments. For example, fluctuation of *o*-TFMBA at 20 to 21 h (Fig. 2) occurred when the generator used for irrigation was accidentally shut off. The major dip in Fig. 3, at 100 to 200 h, occurred when the irrigation system was stopped after an intense thunderstorm event that caused extensive flooding and surface runoff outside the irrigation shed. Furthermore, because no nozzles could offer high uniform irrigation below the 4 mm h^{-1} rate (Hanke et al., 2004), water was applied intermittently under the 1.2 and 2.4 mm h^{-1} infiltration rates in our experimental design. As explained by Gish et al. (2004), this would cause chemical arrival earlier than expected. In Fig. 2, the measured breakthrough pattern under 2.4 mm h^{-1} infiltration had a small initial arrival from 7 to 10 h. Under the 1.2 mm h^{-1} infiltration rate, the measured breakthrough pattern showed two distinct slopes, that is, an initial arrival with less-steep slope from 14 to 40 h (Fig. 3). It is assumed that had irrigation been applied under a true steady-state rate, these initial breakthroughs would not have happened.

THEORY

Characterization of Pore Spectrum of Preferential Flow Pathways

The tails of the tracer BTCs shown in Fig. 1 to 3, as well as those from Kung et al. (2000a) and Jaynes et al. (2001), provide insight into characterizing the pore spectrum of preferential pathways. These tails plotted on a log-log scale are nearly linear and have slopes close to −3. For fully developed laminar flow through a cylindrical capillary tube with radius R (m) under gravitational gradient with negligible entrance-length effect and low Reynolds Number (e.g., <0.1), the analytical solution of mass flux M (mg s^{-1}) of a short chemical pulse by convective transport (i.e., no dispersion) is as follows (see Appendix A for derivation):

$$M(R, t) = 0 \quad for \quad 0 \le t \le \frac{4\upsilon L}{g\ R^2} \qquad [1]$$

$$M(R, t) = \pi\ R^2\ \frac{R^2 g}{8\upsilon}\ C\left[1 - \left(\frac{4\upsilon L}{gtR^2}\right)^2\right] \quad for$$

$$\frac{4\upsilon L}{g\ R^2} + t_p \ge t \ge \frac{4\upsilon L}{g\ R^2} \qquad [2]$$

$$M(R, t) = \frac{2\pi\upsilon L^2}{g} C\left[\left(\frac{1}{t - t_p}\right)^2 - \left(\frac{1}{t}\right)^2\right] \quad for \quad t \geq \frac{4\upsilon L}{g R^2} + t_p \qquad [3]$$

where t is time (s), υ is kinematic viscosity ($m^2 s^{-1}$), L is length of capillary tube (m), g is gravitational constant ($m s^{-2}$), C is input chemical concentration of a pulse ($mg m^{-3}$), and t_p is duration of application of the short chemical pulse (s). These equations indicate that mass flux through a capillary tube is composed of three stages. First, there is no breakthrough when time is less than chemical arrival time, $4 \upsilon L/(g R^2)$. Equation [2] dictates the initial breakthrough of the pulse. Equation [3] describes the stage after water starts to replace the chemical pulse.

When plotted on a log-log scale, the tail of breakthrough pattern of mass flux through a capillary tube described in Eq. [3] also has a nearly linear tail with slope approximately −3. This strongly suggests that the impact of macropore-type preferential pathways can be visualized as that of cylindrical capillary tubes with a spectrum of pore radii. Obviously, cylindrical capillary tubes do not exist in a natural soil profile. Instead, natural pores under field conditions are tortuous with complex pore geometries, often with constrictions along a pathway (Hillel, 1980, p. 185). Results from lab experiments conducted by Dunn and Phillips (1991) showed that, when a pore was made of multiple sections and each section had a different pore size and pore length, an equivalent pore radius, R_{eq}, could represent overall volumetric water flux through the entire pore. For example, if a complex pathway was made of 10 sections, with radii of $R_1, \ldots, R_{10}$ and lengths of $L_1, \ldots, L_{10}$, the R_{eq} of the entire pathway would be

$$R_{eq} = \left(\frac{\sum_{i=1}^{10} L_i}{\sum_{i=1}^{10} \frac{L_i}{R_i^4}}\right)^{1/4} \qquad [4]$$

Because the denominator of Eq. [4] was mainly dominated by the section with the minimum pore radius, R_{min}, the R_{eq} of the entire pore is almost identical to R_{min}. This suggested that, although a preferential pathway can have very complex pore geometry and varying pore radii, volumetric water flux through this pathway is equivalent to that of a cylindrical capillary tube with radius nearly identical to the minimum pore radius of the pathway.

Kung et al. (2000a, 2000b), Jaynes et al. (2001), and Gish et al. (2004) observed very short breakthrough times (i.e., around 15 min) for a chemical to travel approximately 1 m through preferential pathways. This short transit time suggested that the impact of hydrodynamic dispersion within a capillary tube on chemical mixing can be neglected. Convective transport through a preferential pathway with complex pore geometry can be represented by that through a capillary tube with identical equivalent pore radius. When hydrodynamic dispersion is neglected in a saturated capillary tube under steady-state infiltration, the convective chemical transport is also dictated by Eq. [1] to [3]. As a result, the task of quantifying the pore spectrum of complex preferential pathways is significantly simplified by quantifying the pore spectrum of equivalent cylindrical capillary tubes.

To represent a pore spectrum, a mathematical function with proper characteristics must be found. In natural soils, there are lower and upper limits on pore sizes, that is, no soil pores <1 nm, nor >0.1 m. Therefore, a suitable mathematical function to represent the pore-size spectrum must have sharp cut-off points on both ends of a distribution, beyond which the frequency will be zero. This requirement eliminates frequently used functions such as normal and log-normal functions that have long tails. Ju and Kung (1997) proposed a function with sharp cut-off points to characterize the flux distribution of field-scale funnel-type preferential flow. This function to express the frequency of a pore with radius R is as follows:

$$F(R) = AR^{-\alpha} e^{-\beta \times R^{-\gamma}} e^{-\lambda \times R^{\eta}} \qquad [5]$$

The first term on the right-hand side, A, dictates the overall magnitude of pore frequency. The second term with a variable α dictates the overall slope of a frequency distribution between the two cut-off points. This slope reflects the rate of increase of newly activated pores when infiltration rate increases. The third and fourth are exponential terms with variables (β, γ) and (λ, η), which dictate the locations of the cut-off points and how fast the frequency drops to zero on the left and right side of the spectrum, respectively.

If the pore spectrum of macropore-type preferential flow pathways can be represented by this function, the parameters in Eq. [5] must obey a set of soil physics principles. For example, Hutson and Wagenet (1995) hypothesized that, under low infiltration rates, only pathways with smaller pores could be active; furthermore, as the infiltration rate increases, the smaller paths previously active must remain active as some larger paths become active. These hypotheses imply that parameters A, α, and (β, γ) are constant and can be determined at lower infiltration rates, while only (λ, η) vary as the infiltration rate increases. Furthermore, a pore spectrum with certain parameters under an infiltration rate must simultaneously satisfy the water flux as well as the chemical breakthrough pattern. On the basis of these physics principles, a theoretical pattern of spectra was constructed as steady-state infiltration rates increased (Fig. 4). The parameters of these spectra are shown in Table 1. Initially, only pathways with small pores were active when the infiltration rate was low. The parameters A, α, and (β, γ) were determined at this rate. As infiltration rates increased, larger pores became active, and the parameters (λ, η) varied as the location of the cut-off point on the right-hand side of a spectrum moved. In theory, the parameters of Eq. [5] can be defined from a series of tracer BTCs under different steady-state infiltration rates.

Conceptualization of Pore Spectrum of Preferential Flow Pathways

Our BTCs in Fig. 2 and 3, as well as that from Gish et al. (2004) (shown in Fig. 1), were used to find the six parameters of Eq. [5] under three different steady-state infiltration rates. A wide range of values was systematically tested for each parameter in Eq. [5]. At each combination of these parameters, a mass flux breakthrough pattern was calculated by using Eq. [1] to [3]. On the basis of the least-square fitting, many possible combinations of A, α, (λ, η), and (β, γ) were found that could fit the BTCs under the 1.2 mm h^{-1} infiltration rate. Then, each set of A, α, and (β, γ) was used to find new (λ, η) that could fit the BTCs of the higher infiltration rates in Fig. 1 and 2. This process eliminated all possible combinations of A, α, and (β, γ), because they would not simultaneously fit the BTCs under all three different infiltration rates.

However, when more pathways with small pore radii were allowed to become active as the infiltration rates increased, parameters emerged for each BTC. The pore spectra based on least-square curve-fitting are shown in Fig. 5; the parameters of these spectra are shown in Table 2. Breakthrough patterns calculated by using Eq. [1] to [3] from transport through capillary tubes with the fitted pore spectrum are shown as solid

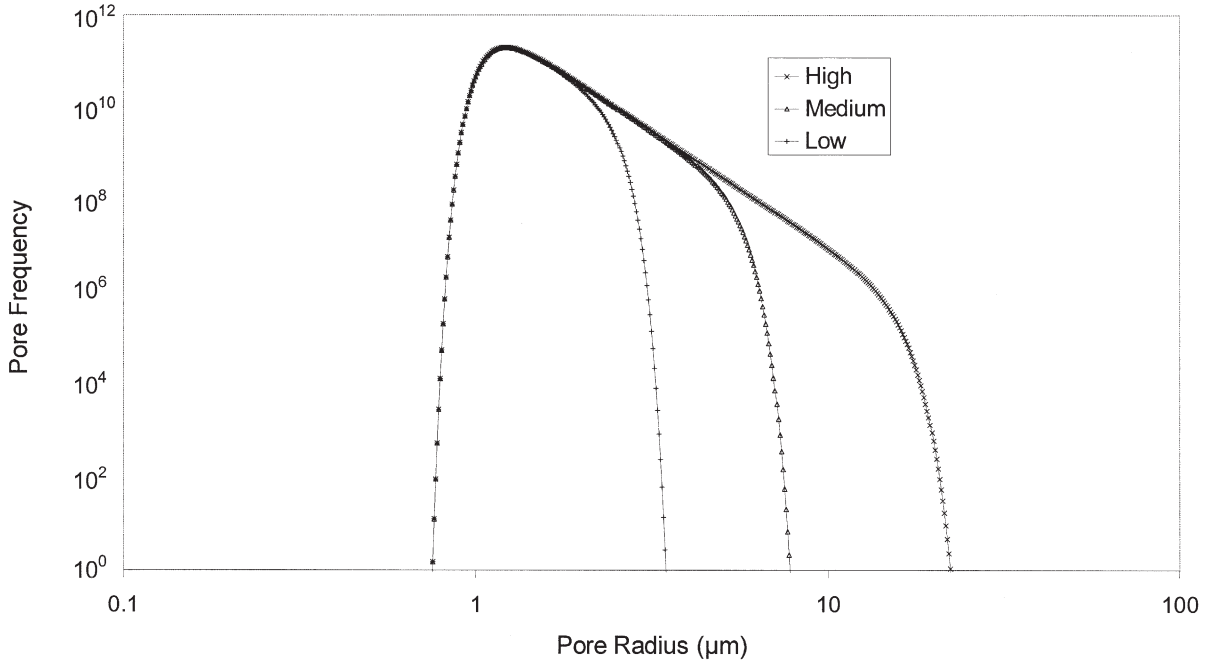

Fig. 4. Theoretical pore spectra based on constraints from conventional conceptualization as steady-state infiltration rates increase.

lines in Fig. 1, 2, and 3. The measured and fitted breakthrough patterns matched well, and each spectrum satisfies both the water infiltration rate and chemical breakthrough pattern. In Fig. 2 and 3, because the initial arrival was caused by our experimental design of intermittent irrigation, the parameters in Table 2 emphasized matching the true arrival of measured breakthrough patterns.

At the high flow rate, both Fig. 4 and 5 have $>10^{11}$ pathways with pore radii approximately 1 μm, and <100 large pathways with pore radii larger than 20 μm. However, how the pore spectrum changes in Fig. 4 and 5 is completely different. According to the conventional concept undergirding the soil characteristic curve, small unsaturated pores have more negative matric potentials and should be filled first. Therefore, only the patterns of pore spectra shown in Fig. 4 are expected because all pathways with small pores must become saturated before water and solute can enter into pathways with larger pores. Patterns based on a wide range of pores becoming hydraulically active simultaneously as the infiltration rates change are counter-intuitive (shown by two spectra labeled with Δ in Fig. 5). These patterns contradicted the hypothesis and conceptualization proposed by Hutson and Wagenet (1995). Unless better physical principles can be found, relaxing the constraints to fit curves immediately jeopardized the validity of our capillary bundle conceptualization.

To conceptualize water movement and contaminant transport through preferential pathways in an unsaturated soil profile, it is important to realize that the derived pore spectra shown in Fig. 5 only reflect the pore frequency of hydraulically active preferential pathways, instead of the actual distribution of saturated pores reflected in the soil characteristic curve. This comprehension is critical because not all water-saturated pores are hydraulically active pathways. Under unsaturated condition, water should indeed first enter the smaller pores. But, most of these smaller pores are water saturated, yet not hydraulically active, and hence are not included in Fig. 5. In the two-domain approach (van Genuchten and Wierenga, 1976), the small, nearly saturated pores that are inactive in solute transport are classified as stagnant pores. Water stored in these pores is considered as immobile water. Initially, it was assumed that such stagnant pores were always stagnant. Later, results from Casey et al. (1998) suggested that the immobile water content changed as the flow velocity varied.

Our results shed light on how stagnant pores could become hydraulically active pathways when infiltration rates change. Gish et al. (2004) showed that no preferential pathways were active under 0.89 mm h^{-1}. Figure 5 demonstrates how more and more preferential pathways become hydraulically active when infiltration rates increase to 1.2, 2.4, and 4.4 mm h^{-1}. The convective transport through preferential pathways is dictated by volumetric flux, which is determined by the fourth power of equivalent pore radius (Jury et al., 1991, p. 76). When a single 10-μm preferential pathway that connects to the soil surface becomes hydraulically active, it can contribute to the flow in 10^4 1-μm preferential pathways, which connect to the 10-μm pathway, but are not directly connecting to the soil surface. This partly explained why preferential pathways with a wide range of pore radii could simultaneously become hydraulically active. Although Fig. 5 showed that new preferential pathways with equivalent pore radii ranging from 0.7 to 6.0 μm became active simultaneously when the rate increased from 1.2 to 2.4 mm h^{-1}, many of the newly activated preferential pathways were already nearly saturated at 1.2 mm h^{-1}. The reason that they did not appear in the previous pore spectrum was because they were water-satiated, but not hydraulically active, under 1.2 mm h^{-1}.

The two pore spectra labeled with Δ in Fig. 5 show the difference between two adjacent spectra. They indicate that (i)

Table 1. Parameters of Eq. [5] for three hypothetical pore spectra based on conventional conceptualization.

	Infiltration rate		
Parameter	**High**	**Medium**	**Low**
A	1.00×10^{12}	1.00×10^{12}	1.00×10^{12}
α	5	5	5
λ	1.00×10^{-7}	1.00×10^{-5}	1.00×10^{-3}
η	6	7	8
β	3	3	3
γ	8	8	8

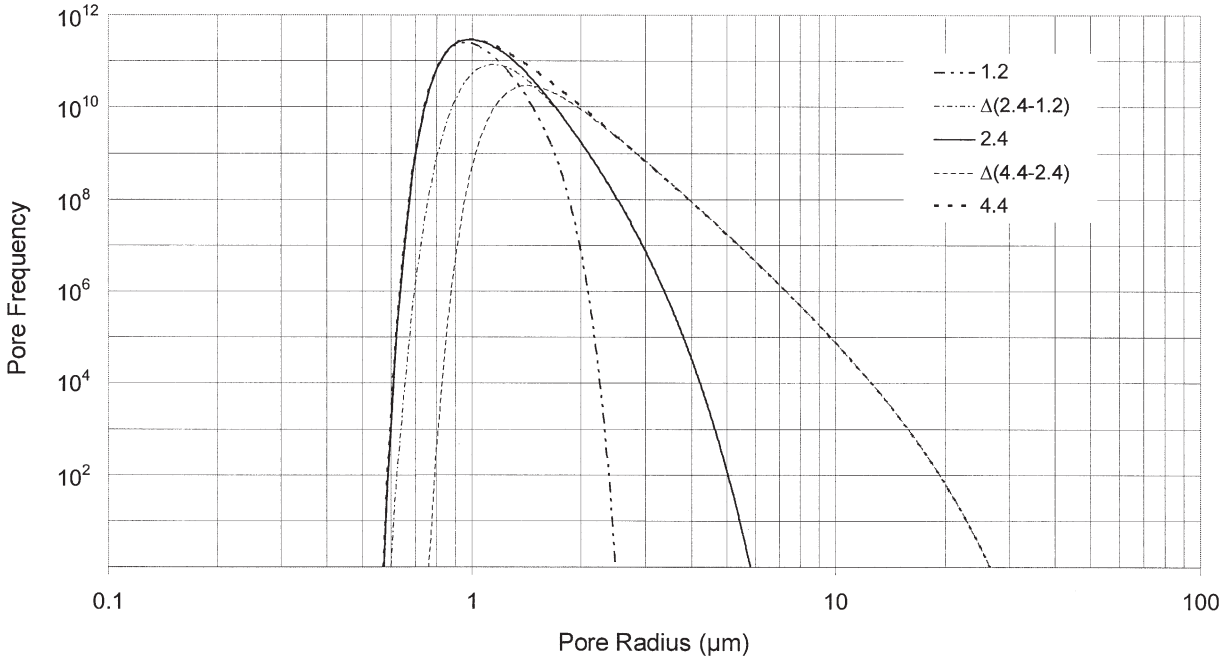

Fig. 5. Pore spectra for three infiltration rates based on fitted parameters after relaxing initial constraints. The spectra labeled with Δ show the difference between two adjacent spectra.

the preferential pathways are made of assemblages of interconnected pores of different sizes; and (ii) within each assemblage, many adjacent preferential pathways are interconnected to form a cluster. Preferential pathways with small pore radii within a cluster become hydraulically active only when their adjacent pathways with larger pore radii become active. When the pathways with larger pore radii are empty, no source of water and solute is available to the pathways with smaller radii within the same cluster. Then, the pathways with smaller radii are essentially stagnant with respect to contaminant transport, although still water-saturated. Because the smaller, nonactive pathways remain nearly saturated, the lateral gradient of matric potential is essentially zero, and the nonactive pathways could exist in equilibrium with the other pathways belonging to an adjacent active cluster. This conceptualization explains why the pathways with small radii in a nonactive cluster would not induce lateral movement from the active pathways in an adjacent cluster.

In short, we propose a new concept to characterize the behavior of field-scale macropore-type preferential pathways and a new approach to quantify their pore spectra. We represent these pathways as assemblages of clustered capillary tubes. The equivalent pore spectrum of these pathways could be represented by Eq. [5]. By conducting a series of steady-state field experiments on tracer breakthrough under different infiltration rates, one can determine the six parameters in Eq. [5] to characterize the equivalent pore spectrum of these pathways. After quantifying the pore spectrum of preferential flow pathways, it becomes more feasible to predict the impact of these pathways on water movement and contaminant transport.

Table 2. Parameters based on best-fit of Eq. [5] to measured breakthrough patterns shown in Fig. 1, 2, and 3.

	Infiltration rate, mm h^{-1}		
Parameter	**4.4**	**2.4**	**1.2**
A	5.17×10^{11}	1.05×10^{12}	1.01×10^{12}
α	7.09	7.13	7.13
λ	0.0119	0.221	0.325
η	1.84	2.76	4.16
β	1.98	2.11	1.99
γ	3.39	6.58	6.58

DISCUSSION

Because volumetric flow is proportional to the fourth power of the pore radius, the smaller soil pores serve as storage and larger pores are conduits for transport pathways. To predict infiltration, aeration, and deep leaching of chemicals, it is necessary to characterize the pore spectrum of larger structural pores that constitute preferential pathways. Nevertheless, since the 1960s, no methodology has been developed to actually measure pore spectrum of a field soil. In our opinion, this is partly because the soil hydraulic conductivity can be used satisfactorily to estimate water flux in the Darcy Law (or Darcy–Buckingham Law) and, on the other hand, the Richards Equation and CDE based on the Darcy water flux can successfully predict chemical transport in unsaturated soils, when by matrix flow is dominant (Cassel et al., 1975; Wierenga et al., 1991; Gish et al., 2004). In the measurement of soil hydraulic conductivity, the contributions from all individual pathways are lumped into a single value under an infiltration rate. Therefore, there is (in this case) no need to characterize the soil pore spectrum.

However, when convective transport through preferential pathways was dominant, the lumped soil hydraulic conductivity became inadequate. To illustrate the intrinsic drawback embedded in using soil hydraulic conductivity, we propose a hypothetical soil profile with preferential pathways made of vertical cylindrical tubes with pore spectrum identical to that shown in Fig. 5. When our hypothetical soil is saturated, the volumetric water flux, V, under unit gradient is

$$V = \sum_{i=1}^{n} \frac{\pi r_i^4 g}{8\upsilon} + \sum_{i=1}^{j} \frac{\pi f_i R_i^4 g}{8\upsilon}$$

where n is the total number of matrix pores, r_i is radius of the ith matrix pore, j is the total number of preferential pathways, and f_i and R_i are frequency and radius of the ith preferential pathway, respectively. The saturated soil hydraulic conductivity of the entire profile is

$$K = \frac{V}{A} = \frac{\pi g}{8\upsilon A} \sum_{i=1}^{n} r_i^4 + \frac{\pi g}{8\upsilon A} \sum_{i=1}^{j} f_f R_i^4 = K_m + K_p$$

where A is the cross-section area of the entire soil profile, K_m is the lumped soil hydraulic conductivity of all soil matrix pores, and K_p is the lumped soil hydraulic conductivity of all preferential pathways.

When preferential pathways were not active, the K_m is indeed adequate to describe a tracer breakthrough pattern measured at a 0.89 mm h^{-1} steady-state infiltration rate on our site (Gish et al., 2004). However, when steady-state infiltration rate increased from 0.89 mm h^{-1} to 4.4 mm h^{-1}, the tracer arrival time drastically shortened from 90 h to 16 min. This was because some preferential pathways with larger pore radii became active as a soil profile became wetter. On the basis of the lumped soil hydraulic conductivity, one would expect that K would increase only about five times when steady-state infiltration rate increased from 0.89 to 4.4 mm h^{-1}. Gish et al. (2004) found that a larger water flux alone was not enough, and an unrealistically large dispersion coefficient was needed to explain the drastic change in tracer arrival time. Under transient conditions, Kung et al. (2000a) observed that four conservative tracers sequentially applied at 0, 2, 4, and 6 h during a 10-h irrigation event had breakthrough times of 238, 102, 42, and 18 min, respectively. In a similar study, Jaynes et al. (2001) demonstrated that the fast arrival through preferential pathways could not be simulated by solving a 1-D CDE where contributions from all active pathways are lumped into a single K.

The two-domain (van Genuchten and Wierenga, 1976) and multiple-domain (Hutson and Wagenet, 1995; Gwo et al., 1995) approaches were proposed to compensate for the intrinsic drawback of lumping contributions from all pathways embedded in the measurement of soil hydraulic conductivity. Because different chemicals were allowed to enter and be transported through different domains, it became possible in these modified approaches that a chemical applied later could exit earlier than another chemical applied first. Similarly, Dagan and Bresler (1979), Van der Zee and van Riemsdijk (1987), Steenhuis et al. (1990), and Toride and Leij (1996) proposed stream tube models, where a soil profile is conceptualized as being made of multiple stream tubes. The adjacent stream tubes can be either independent or interacting. Because each stream tube can be treated theoretically as an independent domain, the essence of stream tube approach is intrinsically similar to that of the multiple-domain approach.

Assume a scenario that (i) our hypothetical soil profile can be delineated into two domains, that is, matrix pore domain and preferential pathway domain; (ii) the lumped soil hydraulic conductivity $K_p = \frac{\pi g}{8\upsilon A} \sum_{i=1}^{j} f_i R_i^4$ of the preferential pathway domain can be accurately measured; and (iii) there is no lateral dispersion between the two domains. Under steady-state condition, the simulated results based on this two-domain scenario will offer a breakthrough pattern made of two distinct peaks (i.e., a lumped soil hydraulic conductivity from each domain would cause a distinct breakthrough peak). In reality, however, convective flow through each ith preferential pathway would cause a breakthrough pattern with a distinct peak. When the j breakthrough patterns are summed together, the overall BTC from this hypothetical profile would show a broad peak similar to that shown in Fig. 1. This mental experiment demonstrates that it is intrinsically wrong to use a single lumped value of soil hydraulic conductivity to predict convective contaminant transport through preferential pathways.

By conducting 1-D numerical experiments, Durner and Flühler (1996) concluded that a continuous pore spectrum must be considered to simulate chemical transport associated with macropores and suggested that multiple-domain approaches could alleviate the drawback associated with single-domain approach. In theory, multiple domains and multiple stream tubes can both eliminate the drawback embedded in the lumped soil hydraulic conductivity. To use these approaches to simulate the breakthrough patterns of four tracers transported under four velocities as observed by Kung et al. (2000a) and Jaynes et al. (2001), it is necessary to divide a soil into four distinct domains. The success of using multiple-domain and multiple-stream-tube models hinges on the accurate measurement of soil hydraulic conductivity for each domain or tube. Because of spatial variability, it is a difficult task to quantify the hydraulic conductivity of field soil even when the soil is treated as a single domain (Biggar and Nielsen, 1976). The task becomes really daunting when attempting to measure hydraulic conductivity for a soil profile that is further divided into multiple domains. Moreover, although studies have demonstrated the usefulness of the multiple-domain and multiple-stream-tube approaches, it has never been rigorously addressed how to define the boundaries among multiple domains or tubes, or whether such boundaries indeed exist. Another main difficulty in using the multiple-domain or multiple-stream-tubes approach is the lack of methodology to deterministically determine the connectivity and lateral mixing among domains or tubes. For example, a chemical could enter the soil surface through 10 initial pathways under a certain infiltration rate and reach the water table through 1000 final pathways. It is almost impossible to deterministically quantify the interaction and connectivity through lateral mixing among the 10 initial pathways and the 1000 final pathways to simulate the chemical transport.

Jury (1982) proposed an alternative stochastic transfer function approach. Instead of measuring the lumped soil hydraulic conductivity, long-term field-scale tracer BTCs were measured and used to estimate the PDF of solute transport. This approach was powerful because the

net effect of how soil pores are naturally divided into domains and whether there is lateral mixing among adjacent domains is automatically reflected in field-scale tracer BTCs. In other words, the essentialness of quantifying pore spectrum to reflect convective transport through individual preferential pathways is implicitly embedded in this approach. However, results from Fig. 1 to 3 show that key physical parameters such as rain intensity would dictate when certain pathways will become hydraulically active. For same amount of net infiltration, two different infiltration rates would cause two completely different breakthrough patterns. Because pore spectrum was not explicitly quantified in the transfer function approach, it is difficult to modify a PDF derived from a specific growing season to simulate a field-scale tracer BTC of another season with identical net infiltration but very different set of boundary conditions.

In our approach, the strengths of the deterministic approach and the transfer function approach were combined. Instead of using water movement to determine the lumped soil hydraulic conductivities K_m and K_p, field-scale BTCs of tracer mass flux were measured with an improved tile-drain protocol under different flow rates. We then used these BTCs as surrogates to quantify pore spectra of active preferential pathways at different infiltration rates. The behavior of fitted pore spectra in Fig. 5 showed that the active soil pores are indeed divided into domains (or clusters). Because no lumping was done in our pore spectrum conceptualization, pores are intrinsically divided into a continuum of domains. As infiltration rate changes, the spectra offer insight on how a new cluster of preferential pathways becomes active. Therefore, quantifying the change of active pore spectra under step-wise small incremental changes of infiltration rates (e.g., every 0.5 mm h^{-1}) could define boundaries among natural pore domains and quantify the interconnectivity of newly activated pathways. This holistic and deterministic approach includes the net effect of (i) when certain preferential pathways will become hydraulically active, and (ii) how soil pathways are naturally divided into domains.

On the surface, it seemed that our approach bypassed the critical issue of interconnectivity among pores because we assumed that all final pathways were independent. However, when mass flux breakthrough patterns under different infiltration rates were measured, the derived pore spectra automatically revealed how the newly activated pathways were interconnected as a cluster (or domain). Therefore, the critical information concerning the interaction and connectivity through lateral mixing among the 10 initial pathways and the 1000 final pathways is intrinsically embedded in our approach. In other words, to quantify the pore spectra served as a new methodology to deterministically determine the connectivity and lateral mixing among domains (or tubes).

The pore spectra derived by our approach can simultaneously satisfy both water movement and solute transport. The soil hydraulic conductivity of preferential pathways, which is critical to all deterministic approaches, is automatically included in a soil pore spectrum (i.e., integrating volumetric water flux across a pore spectrum will yield the net soil hydraulic conductivity of all active preferential pathways under a certain infiltration rate). Therefore, we offered a new method to measure soil hydraulic conductivity of preferential pathways for deterministic approaches. After accurately quantifying a soil pore-size spectrum, one could artificially divide preferential pathways into a fixed number of domains and calculate the soil hydraulic conductivity of each domain according to the need of a practical problem. Therefore, it becomes possible to use multiple-domain or multiple-stream-tube approaches to deterministically predict water flux and contaminant transport through preferential pathways. On the other hand, although the total annual precipitation at a location might be close to a constant, how multiple precipitation events with different intensities and durations are combined for different years would be completely random. Instead of measuring a single PDF to predict long-term behavior of field-scale contaminant transport, one can use information embedded in the soil pore spectra to construct multiple PDFs of the transfer function approach to reflect the impact of different precipitation patterns within a growing reason on chemical transport. Therefore, the usefulness of the transfer function approach can be enhanced after the equivalent pore-size spectra under different rain intensities and durations are quantified.

We proposed an alternative approach to quantify the contribution of macropore-type preferential pathways on water movement and chemical transport. However, Eq. [1] to [3] used in this paper were only for the most simplified case, when hydrodynamic dispersion and chemical adsorption or degradation were all neglected. To use our approach to simulate the transport of reactive chemicals such as pesticides or pathogens such as bacteria and viruses, hydrodynamic dispersion, chemical degradation, and retardation by adsorption must be considered. Under these scenarios, other sets of analytical solutions, such as those derived by Aris (1959), Yu (1981), and Farooq and Karimi (2003), need to be used to replace Eq. [1] to [3]. On the other hand, some preferential pathways such as planar fractures cannot be represented as capillary tubes. Again, other sets of analytical solutions need to be used to replace Eq. [1] to [3]. For example, Tang et al (1981), Sudicky and Frind (1984), Berkowitz and Zhou (1996), and Sun and Buscheck (2003) presented analytical solutions for chemical transport in a single fracture.

SUMMARY

The pore-size spectrum is one of the most important properties of soils. No methodology has been developed to directly characterize the soil pore-size spectrum, especially when macropore-type preferential flow pathways are activated. In the deterministic models, the usage of soil hydraulic conductivity can bypass the need to quantify soil pore-size spectrum. However, the contributions from individual pathways are lumped in the measurement of soil hydraulic conductivity. In our opinion, this may have impeded progress in the conceptual under-

standing and prediction of field-scale contaminant transport through macropore-type preferential pathways.

In this study, we proposed an indirect method to quantify equivalent pore spectrum of preferential pathways to eliminate this bottleneck. We used an improved tile drain monitoring protocol, that is, applying tracer to a narrow strip near the tile line, to accurately measure breakthrough patterns of tracer mass flux. From the tails of these patterns, we found that the impact of preferential pathways on contaminant transport can be represented conceptually as flow through a series of cylindrical capillary tubes. We then proposed a function with sharp cut-off points on both sides of the pore-size distribution to represent the pore spectrum of these tubes. Finally, we used the measured BTCs as surrogates to find the parameters of the proposed function to derive the pore spectrum of preferential pathways.

Our results—based on data best-fitting—showed that the preferential pathways are indeed naturally clustered into domains, and preferential pathways with a wide range of equivalent pore radii could become active when the infiltration rate increases. This suggested that our approach implicitly revealed how pathways were internally connected and interacted. Because the pore spectra derived by our approach simultaneously satisfy both water movement and solute transport, information embedded in pore spectra can be used to (i) measure soil hydraulic conductivities of preferential pathways of different domains for the multiple-domain deterministic models, and (ii) construct multiple PDFs of the transfer function approach to accommodate the impact of different precipitation patterns on contaminant transport through macropore-type preferential flow pathways.

APPENDIX A

Convective Mass Flux of a Short Chemical Pulse through a Capillary Tube without Molecular Diffusion

Derivation

Taylor (1953) first derived analytical equations to calculate averaged chemical concentration during five phases for convective transport of a chemical pulse through a capillary tube under steady-state flow condition without molecular diffusion (i.e., his Eq. [8] for Case A-3). Chemical mass flux at the exit of the tube is the product of chemical concentration and volumetric water flux. However, because both the chemical concentration and the volumetric water flux in a capillary tube can be functions of distance from the pore center, one cannot calculate chemical mass flux at each of the five phases by simply multiplying the averaged chemical concentration and the averaged volumetric water flux. Instead, it is necessary to integrate the local product of chemical concentration and volumetric water flux. Under low Reynolds number (e.g., <0.1) and negligible entrance-length effect, the flow velocity, u (m s^{-1}), within a cylindrical capillary tube under free drain condition is axially symmetric as follows:

$$u = g\,(R^2 - r^2)/(4\upsilon)$$

where R is the radius of the tube (m), r is the distance from the center of the tube (m), υ is kinematic viscosity (m^2 s^{-1}), and g is the gravitational constant (m s^{-2}). The maximum flow velocity, u_{max}, occurs at the center of the tube where $r = 0$. Under steady-state flow condition, the arrival time, t_{ar} (s), required for a chemical to travel from the entrance to the exit of a capillary tube of length L (m) is

$$t_{ar} = L/u_{max} = (4\upsilon L)/(R^2 g)$$

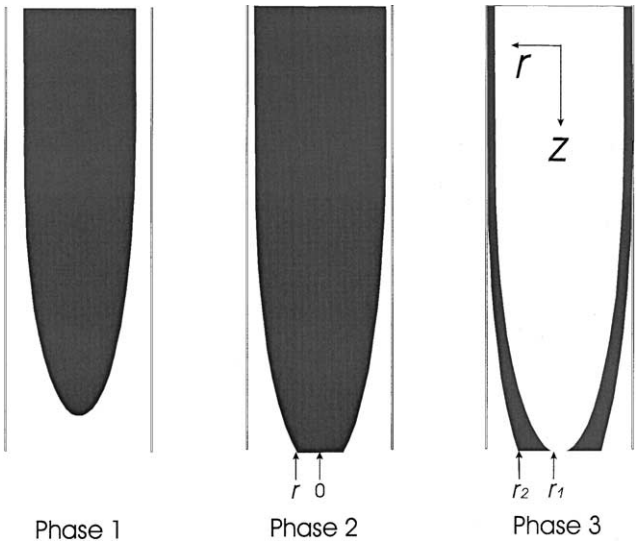

Fig. A1. Three phases of convective transport of a chemical through a capillary tube. r is the distance from the center of the tube (m), r_1 is the location where the new water front reaches the exit, and r_2 is the location where the chemical front reaches the exit.

Phase 1. When time is less than t_{ar}, the chemical front has not reached the exit (see Phase 1 of Fig. A1) and hence, chemical mass flux, MF (mg s^{-1}), in a tube with radius R is zero.

$$M(R, t) = 0 \quad \text{for} \quad 0 \le t \le (4\upsilon L)/(g\,R^2)$$

Phase 2. When time is larger than t_{ar}, the chemical mass flux occurs at the exit. Because local flow velocity where the chemical front reaches the exit is a function of distance from pore center (r) (Phase 2 of Fig. A1), chemical mass flux from a tube with radius R can be calculated by integrating the local product of chemical concentration and volumetric water flux as follows:

$$MF\,(R, r, t) = \int_0^{r(t)} 2\pi r u C_o dr = \int_0^{r(t)} 2\pi r \left(\frac{R^2 - r^2}{4\,\upsilon}\right) g C_o dr$$

where C_o is input chemical concentration (mg m^{-3}) when there is no hydrodynamic dispersion. However, because $ut = L$, the relationship between r and t is

$$ut = \frac{R^2 - r^2}{4\upsilon} gt = L \quad \text{or} \quad r(t) = \sqrt{R^2 - \frac{4\upsilon L}{gt}}$$

Therefore, chemical mass flux becomes a function of time as follows:

$$MF\,(R, t) = \int_0^{\sqrt{R^2 - \frac{4\upsilon L}{gt}}} 2\pi r \left(\frac{R^2 - r^2}{4\upsilon}\right) g C_o dr$$

$$= \frac{2\pi g C_o}{4\upsilon} \int_0^{\sqrt{R^2 - \frac{4\upsilon L}{gt}}} (rR^2 - r^3)\,dr$$

$$MF\,(R, t) = \frac{\pi g C_o}{2\upsilon}\left(\frac{2\,r^2\,R^2 - r^4}{4}\right)\Bigg|_0^{\sqrt{R^2 - \frac{4\upsilon L}{gt}}}$$

$$= \frac{\pi R^4\, g C_o}{8\upsilon}\left[1 - \left(\frac{4\upsilon L}{R^2 gt}\right)^2\right]$$

Phase 3. When a chemical is applied as a short pulse during a steady-state flow condition and t_p is the time of chemical application, the new water front at the center of the tube arrives the exit of the tube at $t = t_{ar} + t_p$. The chemical mass flux at time larger than $t_{ar} + t_p$ is as follows:

$$MF\,(R, r_1, r_2, t) = \int_{r_1}^{r_2} 2\pi r u C_o dr$$

$$= \int_{r_1}^{r_2} 2\pi r\left(\frac{R^2 - r^2}{4\upsilon}\right) g C_o dr$$

where r_2 is the location where the chemical front reaches the exit and where r_1 is the location where the new water front reaches the exit (see Phase 3 of Fig. A1). Both r_1 and r_2 are related to t as follows:

$$\frac{R^2 - r_2^2}{4\upsilon} gt = L \quad \text{and} \quad \frac{R^2 - r_1^2}{4\upsilon} g\,(t - t_p) = L$$

$$r_2 = \sqrt{R^2 - \frac{4\upsilon L}{gt}} \quad \text{and} \quad r_1 = \sqrt{R^2 - \frac{4\upsilon L}{g\,(t - t_p)}}$$

$$MF\,(R, t) = \int_{\sqrt{R^2 - \frac{4\upsilon L}{(t - t_p)}}}^{\sqrt{R^2 - \frac{4\upsilon L}{gt}}} 2\pi r\left(\frac{R^2 - r^2}{4\upsilon}\right) g C_o dr$$

$$= \frac{\pi g C_o}{2\upsilon}\left(\frac{2\,r^2\,R^2 - r^4}{4}\right)\Bigg|_{\sqrt{R^2 - \frac{4\upsilon L}{g(t - t_p)}}}^{\sqrt{R^2 - \frac{4\upsilon L}{gt}}}$$

$$MF\,(R, t) = \frac{2\pi\upsilon L^2\, C_o}{g}\left[\frac{1}{(t - t_p)^2} - \frac{1}{t^2}\right]$$

On the basis of the derived analytical solutions, the overall mass breakthrough pattern of convective chemical transport through a capillary tube without molecular diffusion is made of three phases as shown in Fig. A2.

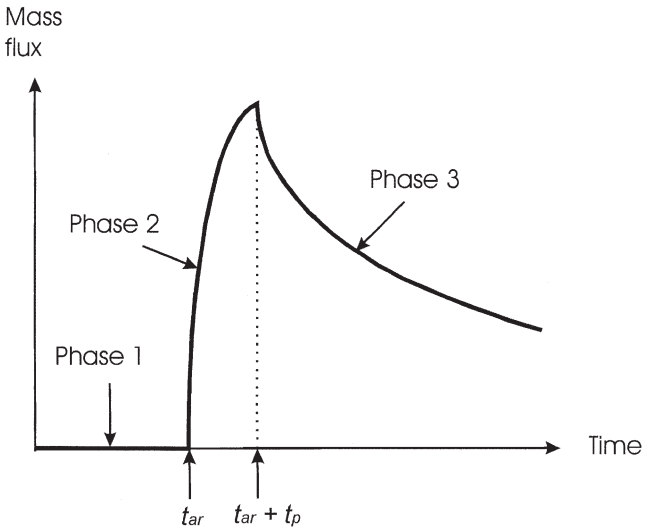

Fig. A2. Typical mass flux breakthrough pattern during the three phases of convective transport of a chemical through a capillary tube.

Discussion

Taylor (1953) first derived analytical equations of averaged chemical concentration for convective transport of a chemical pulse through a capillary tube without molecular diffusion. His derivation was based on an experimental design where a plug of chemical was uniformly distributed at the entrance of a capillary tube at time zero (i.e., A-3 of Fig. 1 on page 189 of his paper). This was because he introduced the chemical into the tube when the flow was stopped. On the basis of Taylor's experimental setup, the total mass entered and transported through a pore with radius R was proportional to the second power of R (i.e., total mass = $\pi R^2 \chi C_o$, where χ is the thickness of the initial uniform plug). This configuration of chemical input was referred to as "slug input" by Gill and Ananthakrishnan (1967). Therefore, the ratio of total mass transported through a 10-μm capillary pore and a 1-μm capillary pore would be $(10/1)^2$ or 100.

In our experimental setup, a chemical pulse was applied under a steady-state flow condition (i.e., a chemical pulse entered a pore while water was flowing). As a result, a chemical does not enter a pore uniformly as a slug. Because the flow velocity is parabolic across the pore radius, much more chemical will enter and be transported through the region near the center of the pore in our case (see Phase 1 of Fig. A1). On the basis of our derivation, the total mass entered a pore with radius R is the summation from three phases as follows:

$$\int_0^\infty MF\,(t)\,dt = 0 + \int_{t_{ar}}^{t_{ar}+t_p} \frac{\pi\, R^4\, g C_o}{8\upsilon}\left[1 - \left(\frac{4\upsilon L}{R^2 gt}\right)^2\right] dt +$$

$$\int_{t_{ar}+t_p}^{\infty} \frac{2\pi\upsilon\, L^2\, C_o}{g}\left[\frac{1}{(t - t_p)^2} - \frac{1}{t^2}\right] dt$$

$$= \frac{\pi\, R^4\, g C_o}{8\upsilon} t_p\left(\frac{R^2\, g t_p}{4\upsilon L + R^2\, g\, t_p}\right) +$$

$$\frac{2\pi\upsilon\, L^2\, C_o}{g}\left(\frac{R^2\, g}{4\upsilon L}\right)^2 t_p\left(\frac{4\upsilon L}{4\upsilon L + R^2\, g t_p}\right)$$

$$= \frac{\pi\, R^4\, g C_o}{8\upsilon} t_p$$

Therefore, according to our experimental setup, the total mass transported through a pore is proportional to the fourth power of pore radius R (i.e., total mass = $\pi R^4\, g\, C_o\, t_p/8\upsilon$). The ratio of total mass transported through a 10-μm capillary pore and a 1-μm capillary pore would be $(10/1)^4$ or 10 000, which is 100 times larger than that based on Taylor's setup.

If a slug of chemical with identical thickness is uniformly distributed near soil surface in all pores at the beginning of an infiltration event, Taylor's derivation should be used to calculate mass flux of chemical transport. However, if a chemical pulse entered the capillary pores under steady water movement, using Taylor's analytical solution would grossly underestimate the total convective chemical transport through the larger capillary pores. When molecular diffusivity is important in laminar flow through capillary tube, dispersion only smears the sharpness of chemical front without altering the velocity field of the flow. Therefore, this assessment of underestimating mass ratio through capillary tubes of different radii by Taylor's derivation is still true when molecular diffusion caused dispersion as a chemical pulse entered the capillary pores under steady water movement.

When a chemical was introduced as a uniform slug, a parabolic flow field within a capillary tube could cause the maximum contact along the surface of a chemical front. In other words, a uniform initial slug input in Taylor's experimental setup ensured the maximum dispersion in the convection–dispersion transport phenomenon. In our experimental setup, more chemical entered through the region near the center of a pore where the stretching caused by a parabolic flow field was small. As a result, chemicals entered the capillary pores through water movement experienced a minimum dispersion effect in the convection–dispersion transport phenomenon. Conventional deterministic models were mainly based on solving Taylor's CDE (i.e., his Eq. [9]). Because chemical entrance into individual pores of different radii with water was not considered in conventional deterministic models, the total convective chemical transport through the larger macropore-type preferential pathways is similarly grossly underestimated by conventional deterministic models. This partly explains why unrealistically large dispersivity is a necessity to use deterministic models to simulate the fast convective transport through preferential pathways such as those observed by Kung et al. (2000a) and Jaynes et al. (2001).

ACKNOWLEDGMENTS

Research was partly supported by USDA-ARS Specific Cooperative Agreement 58-1275-9-094. The views and conclusions contained in this document are those of the authors and should not be interpreted as representing the official policies, either expressed or implied, of the funding agencies. Mention of commercial products is for the reader's convenience and does not constitute endorsement by the authors or their institutions. The authors thank two anonymous reviewers who offered constructive suggestions and comments.

REFERENCES

Anderson, S.H., H. Wang, R.L. Peyton, and C.J. Gantzer. 2002. Estimation of porosity and hydraulic conductivity from x-ray CT-measured solute breakthrough. *In* P. Jacobs (ed.) Applications of computerized x-ray tomography in geology and related domains. Geol. Soc., London.

Aris, R. 1959. On the dispersion of a solute by diffusion, convection and exchange between phases. Proc. R. Soc. London, Ser. A 252: 538–550.

Beauchemin, S., R.R. Simard, and D. Cluis. 1998. Forms and concentration of phosphorus in drainage water of twenty-seven tile-drained soils. J. Environ. Qual. 27:721–728.

Berkowitz, B., and J. Zhou. 1996. Reactive solute transport in a single fracture. Water Resour. Res. 32:901–915.

Biggar, J.W., and D.R. Nielsen. 1976. Spatial variability of the leaching characteristics of a field soil. Water Resour. Res. 12:78–84.

Bouma, J. 1981. Soil morphology and preferential flow along macropores. Agric. Water Manage. 3:235–250.

Casey, F.X.M., S.D. Logsdon, R. Horton, and D.B. Jaynes. 1998. Measurement of field soil hydraulic and solute transport parameters. Soil Sci. Soc. Am. J. 62:1172–1178.

Cassel, D.K., M.T. van Genuchten, and P.J. Wierenga. 1975. Predicting anion movement in disturbed and undisturbed soils. Soil Sci. Soc. Am. J. 39:1015–1023.

Dagan, G., and E. Bresler. 1979. Solute dispersion in unsaturated heterogeneous soil at field scale. I. Theory. Soil Sci. Soc. Am. J. 43:461–467.

Dunn, G.H., and R.E. Phillips. 1991. Equivalent diameter of simulated macropore systems during saturated flow. Soil Sci. Soc. Am. J. 55: 1244–1248.

Durner, W., and H. Flühler. 1996. Multi-domain model for pore-size dependent transport of solutes in soils. Geoderma 70:281–297.

Edwards, W.M., M.J. Shipitalo, L.B. Owens, and W.A. Dick. 1993. Factors affecting preferential flow of water and atrazine through earthworm burrows under no-till corn. J. Environ. Qual. 22:453–457.

Farooq, S., and I.A. Karimi. 2003. Dispersed plug flow model for steady-state laminar flow in a tube with a first order sink at the wall. Chem. Eng. Sci. 58(1):171–180.

Fortin, J., E. Gagnon-Bertrand, L. Vezina, and M. Rompre. 2002. Preferential bromide and pesticide movement to tile drains under different cropping practices. J. Environ. Qual. 31:1940–1952.

Geohring, L.D., P.E. Wright, T.S. Steenhuis, and M.F. Walter. 1999. Fecal coliforms in tile drainage effluent. ASAE Paper No. 99–2203. ASAE, St. Joseph, MI.

Germann, P.F., and K. Beven. 1981. Water flow in soil macropores. I. An experimental approach. J. Soil Sci. 32:1–13.

Gill, W.N., and V. Ananthakrishnan. 1967. Laminar dispersion in capillaries. Am. Inst. Chem. Eng. J. 13(4):801–807.

Gish, T.J., and W.A. Jury. 1983. Effect of plant roots and root channels on solute transport. Trans. Am Soc. Agric. Eng. 26(2):440–444, 451.

Gish, T.J., K.-J.S. Kung, D. Perry, J. Posner, G. Bubenzer, C.S. Helling, E.J. Kladivko, and T.S. Steenhuis. 2004. Impact of preferential flow at varying irrigation rates by quantifying mass fluxes. J. Environ. Qual. 33(3):1033–1040.

Gupta, S.C., A. Bhattacharjee, J.F. Moncrief, and E.C. Berry. 2002. Earthworm species and residue placement effects on macropore characteristics and preferential transport. p. 10. *In* 17th World Congr. Soil Sci., Bangkok, Thailand. 14–21 Aug. 2002. Symp. 1, Paper No. 263.

Gwo, J.P., P.M. Jardine, G.W. Wilson, and G.T. Yeh. 1995. A multiple pore region concept to modeling mass transfer in subsurface media. J. Hydrol. (Amsterdam) 164:217–237.

Hanke, M., D. Perry, K.-J.S. Kung, and G. Bubenzer. 2004. A low intensity, high uniformity water application system. Soil Sci. Soc. Am. J. 68:1833–1837.

Helling, C.S., and T.J. Gish. 1991. Physical and chemical processes affecting preferential flow. p. 77–86. *In* T.J. Gish and A. Shirmohammadi (ed.) Preferential flow. Proc. Natl. Symp., 16–17 Dec. 1991, Chicago, IL. ASAE, St. Joseph, MI.

Hergert, G.W., D.R. Bouldin, S.D. Klausner, and P.J. Zwerman. 1981. Phosphorus concentration—Water flow: Interactions in tile effluent from manured land. J. Environ. Qual. 10:338–344.

Hillel, D. 1980. Fundamentals of soil physics. Academic Press, Orlando, FL.

Hutson, J.L., and R.J. Wagenet. 1995. A multiregion model describing water flow and solute transport in heterogeneous soils. Soil Sci. Soc. Am. J. 59:743–751.

Isensee, A.R., R.G. Nash, and C.S. Helling. 1990. Effect of conventional vs. no-tillage on pesticide leaching to shallow groundwater. J. Environ. Qual. 19:434–440.

Jaynes, D.B. 1994. Evaluation of fluorobenzoate tracers in surface soils. Ground Water 32:532–538.

Jaynes, D.B., S.I. Ahmed, K.-J.S. Kung, and R.S. Kanwar. 2001. Temporal dynamics of preferential flow to a subsurface tile drain. Soil Sci. Soc. Am. J. 65:1368–1376.

Ju, S.-H., and K.-J.S. Kung. 1997. Steady-state funnel flow: Its characteristics and impact on modeling. Soil Sci. Soc. Am. J. 61:416–427.

Jury, W.A. 1982. Simulation of solute transport using a transfer function model. Water Resour. Res. 18:363–368.

Jury, W.A., W.R. Gardner, and W.H. Gardner. 1991. Soil physics. 5th ed. John Wiley & Sons, New York.

Kladivko, E.J., L.C. Brown, and J.L. Baker. 2001. Pesticide transport to subsurface tile drains in humid regions of North America. Crit. Rev. Environ. Sci. Technol. 31:1–62.

Kladivko, E.J., J. Grochulska, R.F. Turco, G.E. Van Scoyoc, and J.D. Eigel. 1999. Pesticide and nitrate transport into subsurface tile drains of different spacings. J. Environ. Qual. 28:997–1004.

Kung, K.-J.S., E. Kladivko, T. Gish, T.S. Steenhuis, G. Bubenzer, and C.S. Helling. 2000a. Quantifying preferential flow by breakthrough of sequentially applied tracers: Silt loam soil. Soil Sci. Soc. Am. J. 64:1296–1304.

Kung, K.-J.S., T.S. Steenhuis, E.J. Kladivko, T.J. Gish, G. Bubenzer, and C.S. Helling. 2000b. Impact of preferential flow on the transport of adsorbing and non-adsorbing tracers. Soil Sci. Soc. Am. J. 64: 1290–1296.

Libardi, P.L., K. Reichardt, D.R. Nelsen, and J.W. Biggar. 1980. Simple field methods for estimating soil hydraulic conductivity. Soil Sci. Soc. Am. J. 44:3–6.

Luxmoore, R.J. 1991. On preferential flow and its measurement.

p. 113–121. *In* T.J. Gish and A. Shirmohammadi (ed.) Preferential flow. Proc. Natl. Symp., Chicago, IL. 16–17 Dec. 1991. ASAE, St. Joseph, MI.

Richard, T.L., and T.S. Steenhuis. 1988. Tile drain sampling of preferential flow on a field scale. *In* P.F. Germann (ed.) Rapid and far reaching hydrological processes in the vadose zone. J. Contam. Hydrol. 3:307–325.

Rodvang, S.J., and W.W. Simpkins. 2001. Agricultural contaminants in Quaternary aquitards: A review of occurrence and fate in North America. Hydrogeol. J. 9:44–59.

Seyfried, M.S., and P.S.C. Rao. 1987. Solute transport in undisturbed columns of an aggregated tropical soil: Preferential flow effects. Soil Sci. Soc. Am. J. 51:1434–1444.

Shaw, J.N., L.T. West, D.E. Radcliffe, and D.D. Bosch. 2000. Preferential flow and pedotransfer functions for transport properties in sandy Kandiudults. Soil Sci. Soc. Am. J. 64:670–678.

Shipitalo, M.J., and W.M. Edwards. 1993. Seasonal patterns of water and chemical movement in tilled and no-till column lysimeters. Soil Sci. Soc. Am. J. 57:218–223.

Stamm, C., H. Flühler, R. Gachter, J. Leuenberger, and H. Wunderli. 1998. Preferential transport of phosphorus in drained grassland soils. J. Environ. Qual. 27:515–522.

Steenhuis, T.S., J.-Y. Parlange, and M.S. Andreini. 1990. A numerical model for preferential solute movement in structured soils. Geoderma 46:193–208.

Sudicky, E.A., and E.O. Frind. 1984. Contaminant transport in fractured porous media: Analytical solution for a two member decay chain in a single fracture. Water Resour. Res. 20:1021–1029.

Sun, Y., and T.A. Buscheck. 2003. Analytical solutions for reactive transport of N-member radionuclide chains in a single fracture. J. Contam. Hydrol. 62:695–712.

Tang, D.H., E.O. Frind, and E.A. Sudicky. 1981. Contaminant transport in fractured porous media: Analytical solution for a single fracture. Water Resour. Res. 17(3):555–564.

Taylor, G.I. 1953. Dispersion of soluble matter in solvent flowing slowly through a tube. Proc. R. Soc. London. Ser. A 219:186–203.

Toride, N., and F.J. Leij. 1996. Convective-dispersive stream tube model for field-scale solute transport: Moment analysis. Soil Sci. Soc. Am. J. 60:342–352.

Van der Zee, S.E.A.T.M., and W.H. van Riemsdijk. 1987. Transport of reactive solute in spatially variable soil systems. Water Resour. Res. 23:2059–2069.

van Genuchten, M.Th., and P.J. Wierenga. 1976. Mass transfer studies in sorbing porous media: I. Analytical solution. Soil Sci. Soc. Am. J. 40:473–480.

Warrick, A.W., and D.R. Nielsen. 1980. Spatial variability of soil physical properties in the field. p. 327. *In* D. Hillel (ed.) Applications of soil physics. Academic Press, New York.

Wierenga, P.J., R.G. Hills, and D.B. Hudson. 1991. The Las Cruces trench site: Characterization, experimental results, and one-dimensional flow predictions. Water Resour. Res. 27:2695–2705.

Williams, A.G., J.F. Dowd, D. Scholefield, N.M. Holden, and L.K. Deeks. 2003. Preferential flow variability in a well-structured soil. Soil Sci. Soc. Am. J. 67:1272–1281.

Woessner, W.W., T. Troy, P. Ball, and D.C. DeBorde. 1998. Virus transport in the capture zone of a well penetrating a high hydraulic conductivity aquifer containing a preferential flow zone: Challenges to natural disinfection. p. 167–174. *In* Proc. Source Water Protection Int., Dallas, TX. 28–30 Apr. 1998. National Water Research Inst., Fountain Valley, CA.

Yu, J-S. 1981. Dispersion in laminar-flow through tubes by simultaneous diffusion and convection. J. Appl. Mech.–Trans. ASME 48: 217–223.

Zehe, E., and H. Flühler. 2001. Preferential transport of isoproturon at a plot scale and a field scale tile-drained site. J. Hydrol. 247(1–2): 100–115.